Journal of Structural Geology 30 (2008) 767–776

Contents lists available at ScienceDirect

Journal of Structural Geology

journal homepage: www.elsevier.com/locate/jsg

Rheology of dolomite: Large strain torsion experiments and natural examples

Claudio Delle Piane*, Luigi Burlini, Karsten Kunze, Peter Brack, Jean Pierre Burg

Geological Institute ETH, Leonhardstrasse, 19/LEB Zurich, CH-8092, Switzerland

ARTICLE INFO

Article history:
Received 5 September 2007
Received in revised form 9 February 2008
Accepted 24 February 2008
Available online 8 March 2008

Keywords:
Dolomite
Calcite
Deformation
Diffusion creep
Grain boundary sliding
Boudins

ABSTRACT

A set of large strain deformation experiments is presented to better constrain the conditions in which grain size sensitive mechanisms are dominant during deformation of dolomite. Experiments were made on an internally heated gas apparatus equipped with torsion facilities. The rheological data set was fitted to an empirical flow law that allows extrapolation to natural conditions. Fabric evolution with increasing strain was investigated by means of optical and electron microscopy (electron backscattered diffraction). Extrapolation of the laboratory data to geologically relevant conditions of temperature and strain rate was tested on a natural case of a deformed dolomite–calcite sequence across the contact aureole of the Adamello pluton (southern Alps, Italy). Both the geological data and the laboratory measurements indicate that at high temperature an inversion of the relative strength occurs between the two carbonates, with calcite being the weak phase at low temperature and dolomite being the weak phase at high temperature.

1. Introduction

Dolomite, $CaMg(CO_3)_2$, is a very common mineral in the Earth's crust comprising about 10% of all sedimentary rocks. Together with calcite, it plays an important role in the dynamics of the upper crust. Yet in comparison to calcite, deformation experiments on dolomite have received little attention, the conditions that favour different deformation mechanisms in dolomite have not been determined and flow laws describing high temperature creep have been only partially reported (Heard, 1976; Davis et al., in press). In addition, previous high temperature experiments on dolomites were restricted to single crystals (e.g. Barber and Wenk, 1979, 2001; Barber et al., 1981) or to coarse-grained rocks, such as Dover plains dolomite or Crevola dolomite, in which the dominant deformation mechanism included twinning and slip with little evidence of grain size sensitive intergranular deformation mechanisms such as grain boundary diffusion or sliding (Neumann, 1969; Heard, 1976; Barber et al., 1994). Only recently, Davis et al. (in press) quantitatively described the mechanics of plasticity and diffusion creep of dolomite based on deformation experiments on natural coarse-grained dolomite marbles and on synthetic fine-grained aggregates. All of the previous experimental work was limited to small amounts of strain due to the coaxial configuration of their deformation apparatus. Previous experimental studies, coupled with microstructural analysis, led to the identification of several intracrystalline mechanisms of deformation (Table 1). Dislocation glide occurs mainly on the *c* plane parallel to the *a* direction but also on the *f* and *r* planes, while mechanical twinning is active on the *f* planes (Higgs and Handin, 1959; Barber and Wenk, 1979; Barber et al., 1981; Wenk et al., 1983).

On the other hand, naturally deformed dolomite shows a variety of deformation features so that interpretation of deformation mechanisms based on microstructural considerations has been difficult and often equivocal (e.g. Newman and Mitra, 1994). For example, White and White (1980) reported a TEM study of relatively fine grained (30 μm) dolomite from the Flinton group, south-east Ontario, which underwent deformation under middle amphibolite facies (400–500 MPa and 600 °C). Based on rheological extrapolation and microstructural observations they concluded that grain boundary sliding accompanied by dislocation creep as the primary intracrystalline deformation mechanism, accommodated large amounts of deformation of the fine-grained dolomite.

Field observations often indicate that dolomite is stronger than calcite-rich rocks. Several authors reported the occurrence of fractured dolomite adjacent to limestone and marble showing evidence of plastic deformation (e.g. Woodward et al., 1988; Erickson, 1994). Early experimental studies performed on coarse-grained dolomite, supported the field observations and reported higher fracture and flow strengths for dolomite than for calcite (e.g. Handin et al., 1967). Heard (1976) extrapolated his experimental results to natural strain rates and reported that at deep crustal conditions the flow strengths are largest for dry dunite and dolomite, followed by dry quartzite, marble and wet quarzite.

* Corresponding author. Present address: CSIRO Petroleum Resources, Australian Resources Research Centre, PO Box 1130, Bentley, WA, Australia. Tel.: +61 8 6436 8716; fax: +41 1 632 1080.
E-mail addresses: claudio.dellepiane@csiro.au (C. Delle Piane), burlini@erdw.ethz.ch (L. Burlini), karsten.kunze@emez.ethz.ch (K. Kunze), peter.brack@erdw.ethz.ch (P. Brack), jean-pierre.burg@erdw.ethz.ch (J.P. Burg).

0191-8141/$ – see front matter © 2008 Elsevier Ltd. All rights reserved.
doi:10.1016/j.jsg.2008.02.018

Table 1
Slip and twinning systems of dolomite (modified after Leiss and Barber, 1999)

Slip and twinning systems of dolomite	
c-slip	$(0001)\langle 2\bar{1}\bar{1}0\rangle$
f-slip	$\{\bar{1}012\}\langle 2\bar{2}01\rangle$
r-slip	$\{10\bar{1}4\}\langle \bar{1}2\bar{1}0\rangle$
f-twinning	$\{01\bar{1}2\}\langle 0\bar{1}11\rangle$

1.1. The Adamello example

The Adamello pluton is the largest Tertiary intrusion in the Alps and is located north of Brescia (northern Italy). It was emplaced at shallow levels into the southern Alpine crystalline basement and its Permo–Mesozoic sedimentary cover. Inside a narrow border zone and generally at distances <1500 m from the igneous contacts, the country rocks have been subject to thermal alteration during magma emplacement. Peak contact-metamorphism estimates yield temperatures of 600–650 °C along contacts with intermediate to acidic magmatic rocks and between 850 and 900 °C along contacts with mafic rocks (Callegari and Brack, 2002; Matile and Widmer, 1993; Schmid, 1997).

Marbles of different composition and degrees of purity (see Schmid and Flammer, 2002; Berger and Herwegh, 2004) are found in contact with plutonic rocks along the southern border of the Adamello intrusion, and more precisely, in the surroundings of its oldest part, the Re di Castello pluton.

Dolomite marbles and cross-cutting hydrothermal veins show high-temperature, syn-intrusive deformation features (e.g. Brack, 1983) in the innermost part of the contact aureole (see Fig. 1 for exact location). Folds and boudins found in several outcrops at small distance (70 ± 10 m) from the contact with the pluton indicate that calcite behaved as the strong phase relative to dolomite at the time of deformation (Fig. 2). Ptygmatic folds are characterised by a large ratio of amplitude to wavelength, and are formed by highly plastic ductile deformation. They generally represent conditions where the folded material is of a higher viscosity than the surrounding medium (e.g. Ramsay and Huber, 1983). Boudins show different geometries with pinch and swell structures (Fig. 2c) and necked profiles (Fig. 2d) with calcite showing a more viscous behaviour than the dolomitic matrix. Considering a temperature of the intruding rocks of 850 °C, and a distance from the contact of approx. 70 m, the thermal model of Matile and Widmer (1993) indicates that the marbles underwent temperatures of approx. 700 °C. A chemical and microstructural characterization of dolomite marbles from this area is given in Delle Piane et al. (2007).

The field observations described above cannot be explained with the known rheological data from experiments on calcite and dolomite and contradict the assumption that dolomite is always stronger than calcite (e.g. Heard, 1976). Motivated by these occurrences, we undertook an experimental study to better constrain the rheology of dolomite and define its relative strength compared to calcite over a wide set of temperature and strain rate.

2. Sample preparation and experimental methods

2.1. Starting material

We used synthetic aggregates made from pure dolomite powder, which was obtained by milling a commercial natural dolomite (Microdol Super provided by Alberto Luisoni Mineralstoffe, Switzerland) for several hours (Herwegh et al., 2003).

The grain size of the starting powder was determined using laser particle analysis, which revealed a three-dimensional particle distribution ranging between 0.4 and 15 μm and a mean of approximately 4 μm (Fig. 3). X-Ray fluorescence and single-point electron microbeam analyses proved that the dolomite powder is extremely pure, with almost stochiometric composition (Table 2).

2.2. Room-temperature uniaxial press

Before cold-pressing, the loose powder was dried for at least 24 h in an oven at 120 °C. The powder was cold-pressed into cylindrical stainless steel canisters with an internal diameter of 5.1 cm, length of 20.3 cm, and volume of approx. 415 cm^3, by stepwise filling and pressing of small portions (approx. 20 g) of material. This procedure was designed to eliminate the effect of pressure shadow development and guarantees the homogeneous packing of the powder along the canister length. To avoid excessive

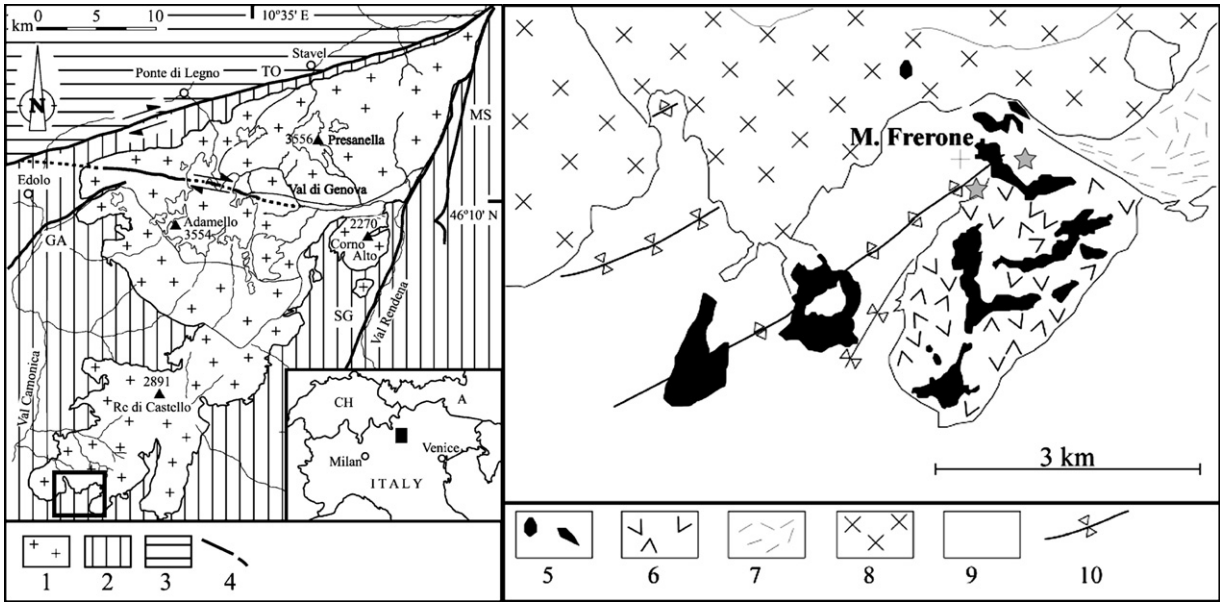

Fig. 1. Geological sketch of the Adamello pluton (redrawn after Di Toro and Pennacchioni, 2004 and Brack, 1983). (1) Composite Adamello batholith; (2) basement and cover of the southern Alps; (3) Austroalpine nappes; (4) major tectonic lines. Right sketch represents an enlargement of the black box in the left map: (5) gabbros and diorite; (6) leucoquarzite; (7) Blumone complex; (8) tonalites; (9) Triassic sediments; (10) major folds. The two stars indicate the location of the structures described in Fig. 2; UTM coordinates 45°56′58.60″N, 10°24′39.70″N.

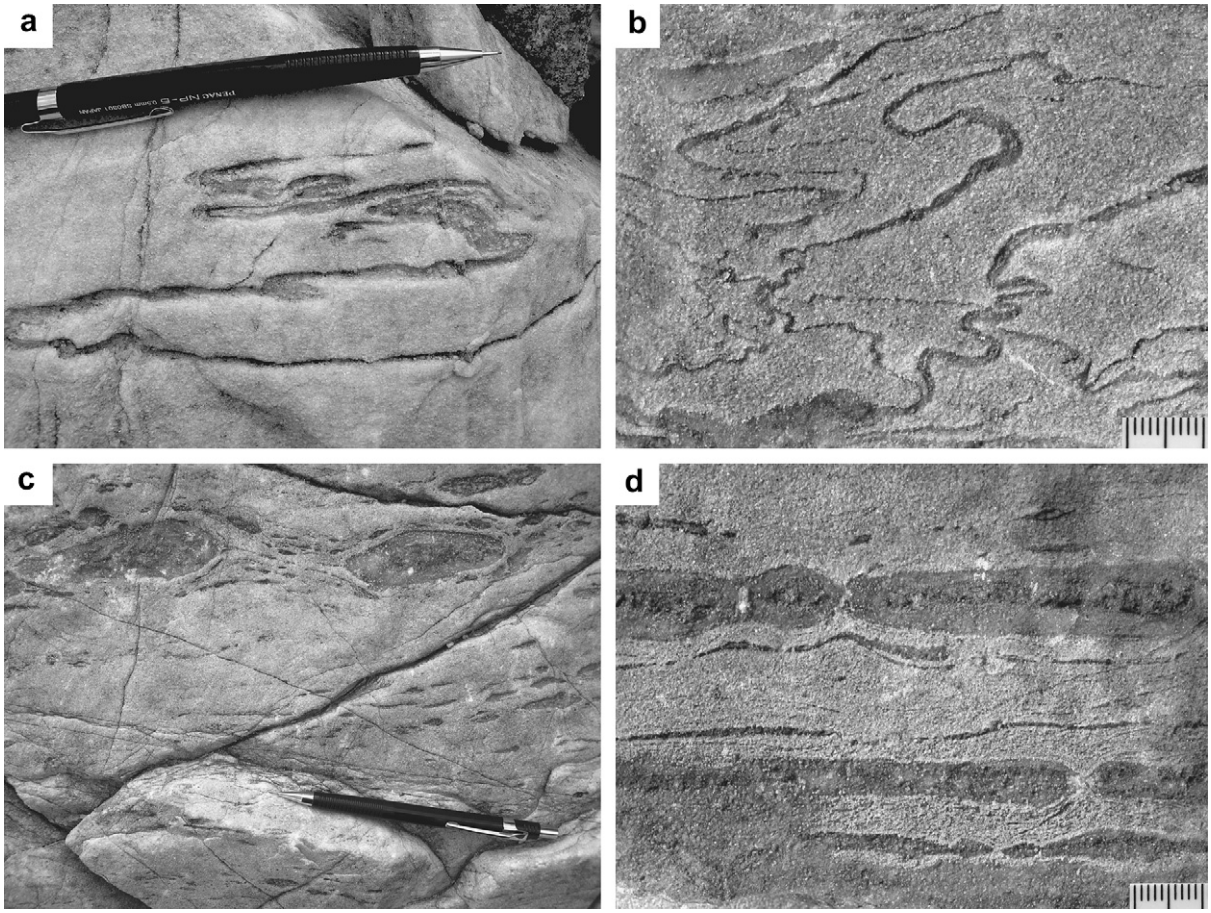

Fig. 2. Ductile deformation in the Mt. Frerone area: outcrops of Dolomia Principale. (a,b) Ptygmatic folds, in this case calcite is the folded material and dolomite the surrounding medium. (c,d) Boudins, calcite shows a more viscous behaviour relative to the dolomitic matrix.

pressure of CO_2 during the following hot-pressing, a small volume of loose sand (Fontainebleau sand) with a porosity of approx. 30% was poured in the top and bottom parts of the canister. This acted as a sink volume, where the CO_2 liberated from the decarbonation of dolomite migrated. The pressing was done with an Enerpac-H-Frame 50-t-press up to a maximum load of 40 t, corresponding to a stress of 200 MPa. The cold-pressed samples were stored at 120 °C until the canisters were sealed by welding. Finally the cylinders were sandblasted in order to remove the surface rust before the hot-pressing.

2.3. High-temperature isostatic pressing

The cylinders were hot isostatically pressed (HIP) using a large volume internally heated argon gas apparatus (Abra) at the Institute of Metallurgy, ETH Zürich. The 18 h HIP conditions were: temperature 700 °C, isostatic pressure of 170 MPa. The cylinders were then cut and cylindrical cores with diameters of 10 and 15 mm and lengths of 10 mm were drilled out of the pressed material. These cores were used to prepare thin sections and samples for deformation experiments. XRF analyses reveal that the

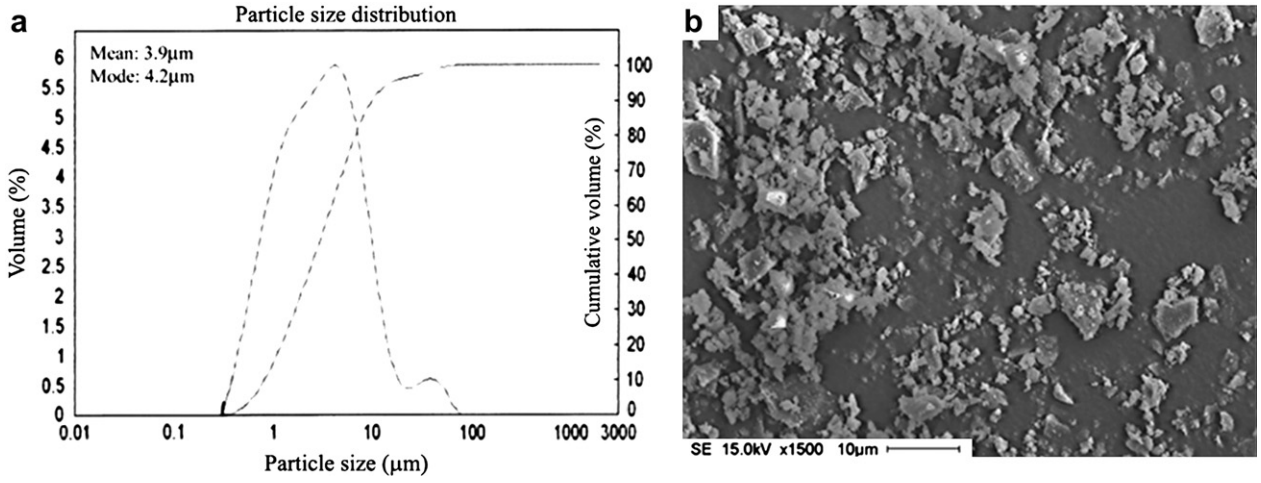

Fig. 3. (a) Particle size distribution from laser particle analysis of the dolomite powder. (b) Secondary electron image of the starting material.

Table 2
Major element analysis on different samples of the dolomitic powder (in wt. %)

	Microprobe				XRF
CaO	29.39	29.26	29.6	29.66	30.35
MgO	21.92	21.54	21.55	21.64	19.92
MnO	0.09	0	0.14	0	0.00
FeO	0.059	0.021	0.10	0.09	0.00
Total	51.45	50.82	51.39	51.39	50.27
LOI[a]					47.07

[a]LOI, loss of ignition.

HIPped material does not contain any contamination from the steel canister.

2.4. Deformation apparatus and experimental techniques

Torsion experiments were performed in an internally heated gas medium (argon) deformation apparatus equipped with a torsion set-up (Paterson and Olgaard, 2000).

Before each run the samples were sandwiched between 3 ± 0.2 mm thick solid alumina spacers; additional alumina and zirconia pistons guarantee a good thermal profile along the sample length. The assembly was then inserted into a pure iron jacket of 0.25 mm wall thickness and 15 mm diameter in order to isolate the sample from the confining gas medium. For the 10 mm diameter samples, the jacket was swaged down to 10 mm in the central part. This resulted in local thickening of the jacket up to a maximum thickness of 0.4 mm.

The temperature distribution inside the furnace was regularly calibrated so that the thermal profile was constant (within ± 1°K) along the sample length. Temperature during the experiments was monitored using a K-type thermocouple placed at about mm from the top of the samples.

Constant displacement rate experiments were performed at 600, 650, 700, 750 and 800 °C, with shear strain rates between 1×10^{-6} s^{-1} and 6×10^{-4} s^{-1} at 300 MPa confining pressure (Table 3).

The measured torque (M) was converted into shear stress (τ) using the equation:

Table 3
Sample geometry and experimental conditions for the runs on synthetic dolomite

Sample no.	D (mm)	L (mm)	T (°C)	Shear strain γ	Strain rate (s^{-1})	Comments
Hdol_1	9.91	9.45	800	~1.2	1×10^{-4}	
Hdol_2	9.91	9.31	800	~7	3×10^{-5}–4.5×10^{-4}	Rate stepping
Hdol_3	15.05	9.99	800	~5	3×10^{-4}	
Hdol_4	15.04	9.71	700	~0.17	3×10^{-4}	
Hdol_5	9.91	11.47	700	~6	1×10^{-5}–3×10^{-4}	Rate stepping
Hdol_6	9.9	8.53	700	–	3×10^{-4}	
Hdol_7	9.9	11.68	700	~3	1×10^{-5}–3×10^{-4}	Rate stepping
Hdol_8	15.04	10.21	800	~3.5	1×10^{-5}–6×10^{-4}	Rate stepping
Hdol_9	9.9	11.28	700	~6.5	9×10^{-6}–2×10^{-4}	Rate stepping
Hdol_10	9.9	11.01	700	~8	3×10^{-6}–2×10^{-5}	Rate stepping
Hdol_11	9.9	11.43	700	1.1	1×10^{-4}	
Hdol_12	9.9	10	700	~4	1×10^{-4}	
Hdol_13	9.9	10	650–750	~2	1×10^{-5}–2×10^{-4}	T and Rate stepping
Hdol_14	9.9	10	600	0.02	1×10^{-6}–1×10^{-5}	Rate stepping
Hdol_15	9.9	10.04	650	0.35	1×10^{-5}–3×10^{-5}	Rate stepping
Hdol_16	9.9	10.03	750	0.8	1×10^{-5}–6×10^{-4}	Rate stepping
Hdol_16	9.9	10.03	725	1.2	1×10^{-4}–6×10^{-4}	Rate stepping
Hdol_17	9.9	10.03	600–650	–	1×10^{-6}–1×10^{-5}	T and Rate stepping
Hdol_18	9.9	10.02	650	0.16	1×10^{-6}–3×10^{-5}	Rate stepping
Hdol_19	9.9	10.04	725	10	3×10^{-4}	

D, diameter; L, length. All experiments performed at a confining pressure of 300 MPa. Intervals indicate runs with stepping of shear strain rate and/or temperature.

$$\tau = \frac{4[3 + (1/n)]M}{\pi d^3} \quad (1)$$

where n is the stress exponent and d is the diameter of the sample (Paterson and Olgaard, 2000), assuming a constant rheology throughout the sample.

The experimental data were analyzed by assuming a flow law of the form:

$$\dot{\gamma} = A\tau^n d^{-m} \exp\left(\frac{-Q}{RT}\right) \quad (2)$$

where $\dot{\gamma}$ is the shear strain rate, τ is the shear stress, d is the grain size, Q is the activation energy, T is the absolute temperature, R is the gas constant, A is a material dependent parameter, and n and m are stress and grain size exponents, respectively.

The stress exponent was determined from the strain rate stepping in a single experiment (Fig. 5c) as well as data from different constant strain rate runs using the relationship:

$$n = \frac{\Delta \ln \dot{\gamma}}{\Delta \ln M} \quad (3)$$

The apparent activation energy Q (Fig. 5b) was established from torque data at different temperatures using the equation:

$$Q = nR\frac{\Delta \ln M}{\Delta(1/T)} \quad (4)$$

The value of the pre-exponential term A as well as that of the grain size exponent m was obtained by fitting the experimental data to the flow law (Eq. (3)) using a non-linear least square regression.

The majority of the experiments were performed in a closed system, using impermeable Al_2O_3 discs placed at the extremities of the specimen to seal the assembly. Such a configuration assures that the dolomite remains in its stability field during the high temperature tests once a small amount of dissociation occurs. As the fluid phase was not escaping, the thermal decarbonation reaction $CaMg(CO_3)_2 \Leftrightarrow CaCO_3 + MgO + CO_2$ was at equilibrium after only a trace of reaction occurred and CO_2 pressures between 1 and approx. 70 MPa (Fig. 9) were building up at temperatures between 600 and 800 °C, respectively (Goldsmith, 1959). SEM-EDS analysis did not reveal reaction products, confirming the good quality of the jacket sealing. A few high temperature tests ($T = 800$ C) were run in vented conditions to investigate the influence of the decarbonation reaction on the deformation behaviour of fine-grained dolomite. Permeable discs of Al_2O_3 with an open porosity of 20–30% placed at extremities of the samples guaranteed good drainage of the fluid phase to the atmosphere.

2.5. Microstructural analysis

Crystallographic preferred orientations (CPO) were analysed using a Camscan CS 44 LB scanning electron microscope (SEM) equipped with a TSL Digiview EBSD attachment. Flat surfaces near the tangential plane to the cylindrical specimens were ground and polished to 0.25 μm using diamond paste on a paper lap, and subsequently chemically–mechanically polished using colloidal silica suspension fluid for several hours. A thin layer (<4 nm) of carbon coating was applied to improve the electrical conductivity of the sample surface and avoid charging problems. The samples were then glued on the sample-holder and connected to the ground with conductive silver paint. The polished specimen surface was inclined at 20° to the incident beam and electron backscatter diffraction patterns were automatically collected from sampling areas of approx. 300 × 300 μm with a step size of 2 μm and automatically indexed using the commercial TSL software OIM at a rate of approx. 10 indexed patterns per second. The following analysis was carried

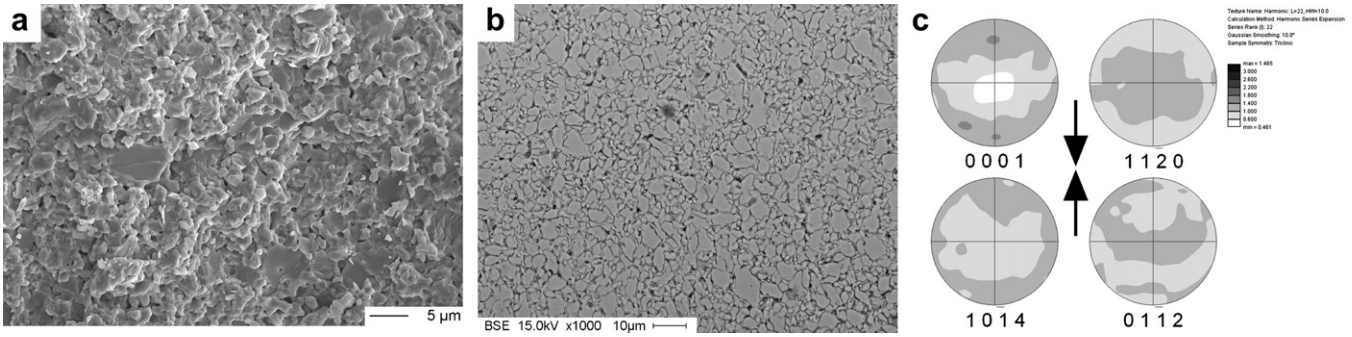

Fig. 4. Microstructure of the HIPped dolomite. (a) Secondary electron image of a broken surface. (b) BSE image of a polished and etched surface, grain boundaries are clearly visible. (c) CPO of the starting material from approx. 1500 sampled grains. Density plots (equal-area projection, upper hemisphere of (c), and axis as well as *r* and *f* poles) with the direction of principal stress during cold-pressing indicated by the black arrows.

out only on data with a high reliability (confidence index >0.1). Contouring of the discrete data was carried out by smoothing with 10° Gaussian width.

3. Results

3.1. Starting material (hot-pressed)

The HIP process resulted in a homogeneous, well-compacted dolomite aggregate with homogeneous texture. The porosity of the samples was estimated using the bulk volume (calculated from the radius and length of each specimen) versus the volume measured using a helium pycnometer (AccuPyc 1330). The difference between the two measurements gives the pore volume, the interconnected porosity can then be calculated as:

$$\phi = \frac{V_p}{V_b} \times 100 \quad (5)$$

where ϕ is the porosity (in %) V_p is the pore volume and V_b is the bulk volume. The density of the fabricated material is

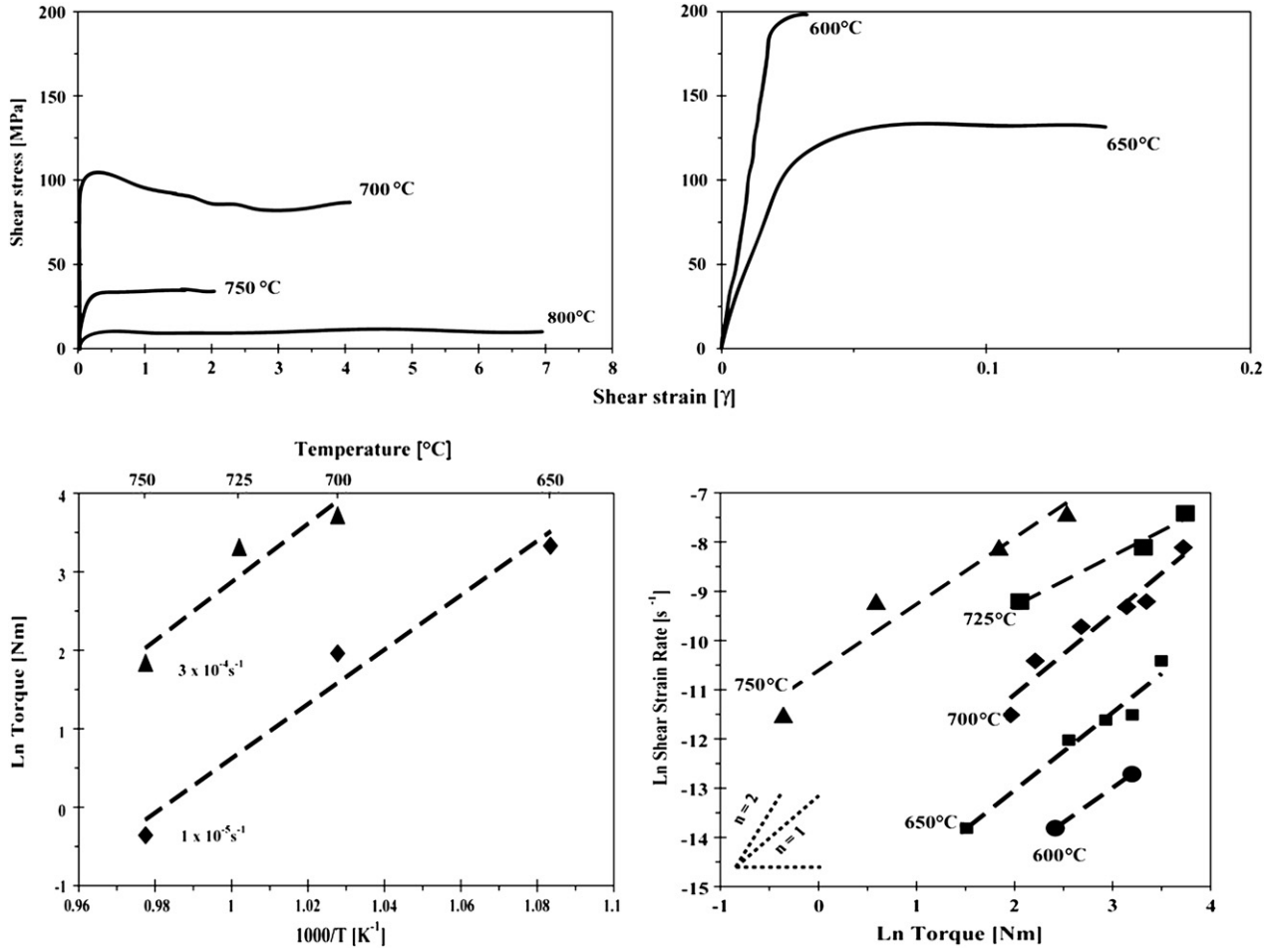

Fig. 5. Selected experimental data of synthetic dolomite. (a) Shear stress versus shear strain curves for constant strain rate experiments conducted at different temperatures. Due to the very slow strain rates applied in experiments run at the 600 and 650 °C, only small amounts of shear strain were attained. The mechanical data for higher temperature experiments indicate a strain-independent value of flow stress. We therefore assumed that the experiments performed at low temperatures are representative of the mechanical steady-state. (b) Temperature sensitivity of the applied torque for different strain rates. Semi-log plot used to derive the activation energy *Q* of the power law. (c) Strain rate sensitivity of the applied torque: the slope of the lines in double log plot gives the stress exponent *n* of the flow law at several temperatures.

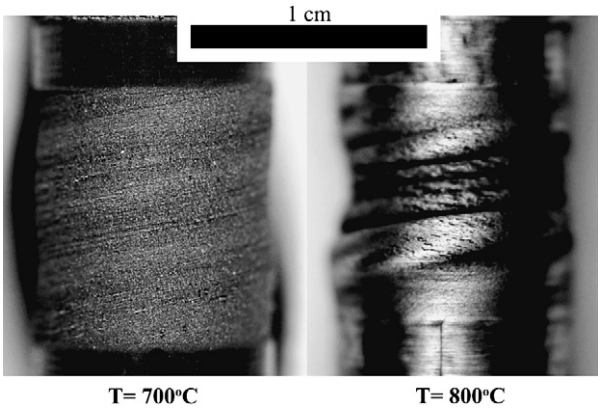

Fig. 6. Deformed samples still surrounded by the iron jackets. Left sample (H_dol5) has been twisted up to a shear strain of $\gamma = 6$ at 700 °C while the specimen on the right underwent a shear strain $\gamma = 7$ at temperature of 800 °C. Note different strain distribution on the sample scale.

2780 kg m^{-3}, corresponding to ~97% of the theoretical value for pure dolomite. The HIPped material has therefore a porosity of ~3%.

Backscatter electron (BSE) images obtained from the SEM CamScan CS-44 LB (acceleration voltage 15 keV, 20–14 mm working distance, and ~4 nA beam current) were processed with ImageTool after manually tracing the grain boundaries and were used to estimate the grain size of the HIPped material. Best results were obtained after applying the two-step etching method as described by Herwegh (2000); the analysis revealed an average value of 4.2 μm for the grain size and 1.7 for the aspect ratio in the non-deformed samples.

The hot-pressed material revealed a weak preferred orientation of the dolomite crystals most likely inherited from the uniaxial cold-pressing stage of preparation (Fig. 4). Specifically, the *c*-axes form maxima near the compression direction.

3.2. Experimental results

About 20 deformation tests were performed to determine the dependence of the shear strength of fine-grained dolomite on strain rate and temperature (Table 3).

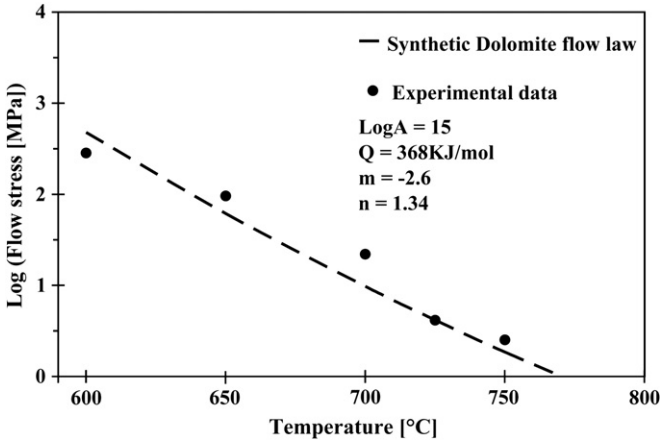

Fig. 7. Experimental data for synthetic dolomite compared to the flow law obtained from non-linear least-square regression for a fixed strain rate of 1×10^{-5} s^{-1}. The flow law obtained from the regression of the experimental data well describes the observed mechanical behaviour at the different temperatures. Best fit flow law parameters are reported in the figure and text.

3.2.1. Mechanical data

Using the analysis described above we obtained the following flow law for fine-grained dolomite (Fig. 7):

$$\dot{\gamma} = 10^{15\pm0.4} \times \tau^{1.3\pm0.2} \times d^{-2.6\pm0.2} \times \exp\left(\frac{-368 \pm 25 \text{ kJ mol}^{-1}}{RT}\right) \quad (6)$$

Strain rate stepping tests at different temperatures show fairly constant stress sensitivity with an average stress exponent of 1.3 ± 0.2 (Fig. 5c), independent of the amount of finite deformation. Temperature stepping tests at constant angular displacement rate were also carried out to evaluate the temperature sensitivity of the dolomite aggregate and yielded a value of 368 ± 25 kJ mol^{-1} for the apparent activation energy *Q*.

At 800 °C the strength of the synthetic dolomite is comparable with that of the iron jacket, the recorded torque is at the limit of resolution of the internal load cell and therefore results in a very noisy signal. Therefore, we did not consider the mechanical data at 800 °C in the data regression. At this temperature, high strain experiments showed a heterogeneous strain distribution along the sample length (Fig. 6) probably driven by ductile instabilities due to some imperfections of the iron jacket itself or to locally very high

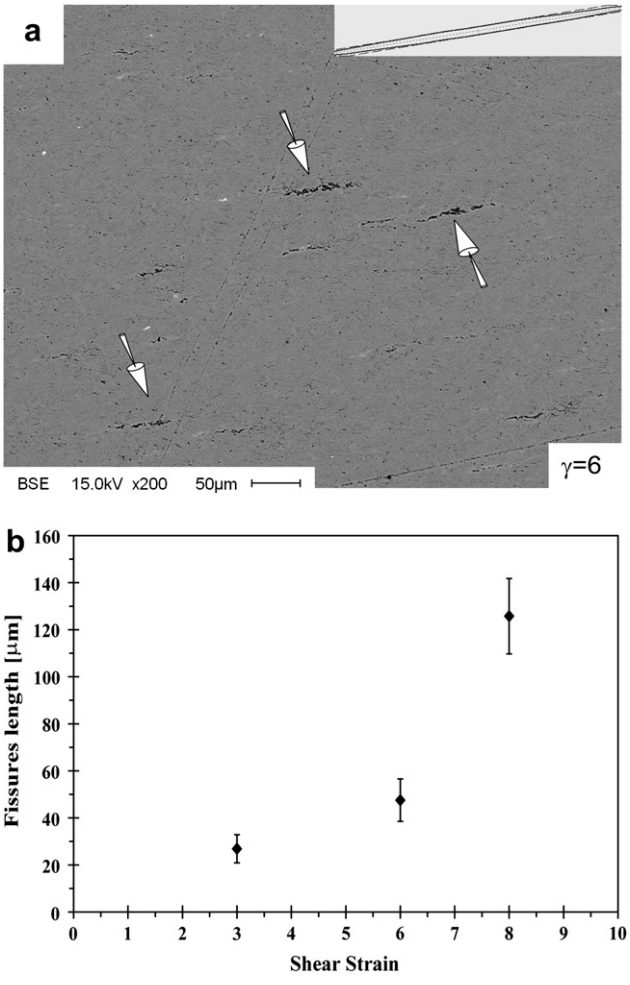

Fig. 8. (a) SEM image in back scattered electron mode illustrating the geometries of cavities from a twisted sample, deformed up to shear strain of 6. Upper right corner represents the strain ellipse at the corresponding finite strain. (b) Average fissure length as a function of shear strain. Ten to 20 fissures measured per data point. The error bars represent the standard deviation of the measured population. The length of each cavity is measured as that of a straight line connecting the two opposite edge tips of a fissure.

CO_2 pressure within the samples, as well as chemical impurities of the cations and of the CO_2.

The experiments performed in vented conditions developed a thin layer of reaction products at the top and bottom sample spacer interfaces. Even for high strain experiments (i.e. long duration) the reaction zones are very narrow, never exceeding ~40 μm in thickness (Fig. 10). The very small grain size of the synthetic aggregate appears to be very effective in trapping the CO_2 generated from the decarbonation reaction. In contrast with what is observed in coarse-grained natural dolomite deformed during reaction (Delle Piane et al., 2007), the reaction layers in the synthetic aggregate do not act as zones of weakness and do not seem to affect the overall distribution of strain at the sample scale.

3.2.2. Microstructures

Optical thin sections (approx. 10 μm thick) were prepared from cuts parallel to the torsion axis and tangential to the cylindrical surface (the "longitudinal tangential" position of Paterson and Olgaard, 2000). Such sections contain the direction of shear displacement and best illustrate the effects of the shear strain. Given the small grain size of the material, optical microscope observations only gave a first qualitative insight to the microstructures. A more detailed analysis of the grain size evolution was undertaken on polished and etched surfaces of the deformed samples observed by SEM BSE imaging.

In samples deformed at 700 °C the grain shape does not differ from that of the starting material maintaining an aspect ratio of 1.7 ± 0.5.

At temperatures higher than 700 °C the grain shape is significantly different from that of the starting material. A representative sample Hdol_19 deformed up to $\gamma = 10$ at 725 °C shows a marked grain flattening resulting in an average aspect ratio of 2.52 with the long axis of the grains obliquely oriented to the sense of shear.

We observed a slight change in aspect ratio to 1.9 ± 0.5 in the specimens deformed to higher strains at 800 °C, but no major change in grain size is observed (Fig. 11), the average value shifts from 4.2 μm in the non-deformed samples to 5.2 μm in a sample deformed up to $\gamma = 7$.

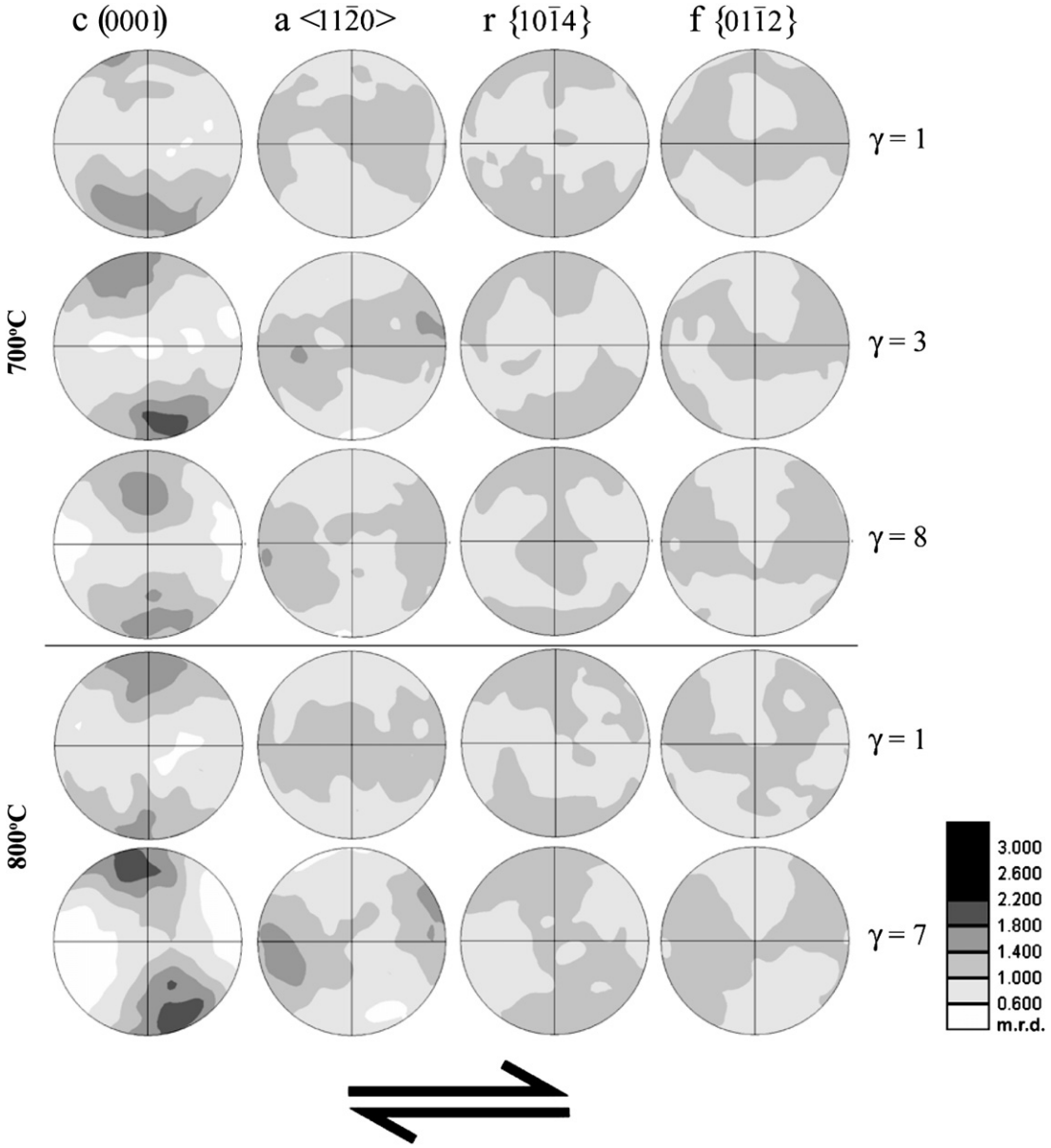

Fig. 9. CPOs of deformed fine grained dolomite as a function of strain obtained from automated EBSD analyses.

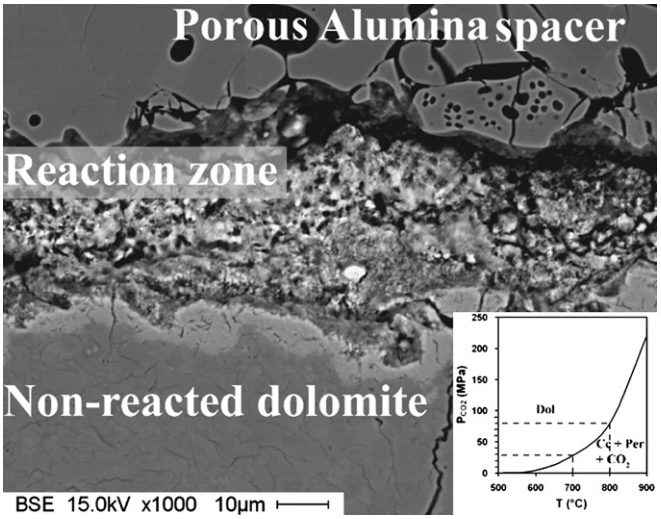

Fig. 10. SEM image in back scattered electron mode of a sample deformed at 800 °C. The porous alumina spacer on top of the sample allows the drainage of fluids released from the decarbonation reaction (1); as a consequence a thin layer of newly formed calcite and periclase grains develops at the sample–spacer interface. Inset, phase diagram (re-drawn after Goldsmith, 1959) illustrating the relationship between equilibrium CO_2 pressure and temperature for the decarbonation reaction of dolomite.

High strain experiments performed at temperatures of 700 °C show distinct cavities systematically oriented parallel to the maximum stretching axis of the finite strain ellipse. The length and angle to the shear zone boundary of these cavities is proportional to the finite amount of strain (Fig. 8b).

3.2.3. Crystallographic preferred orientation

EBSD analysis from samples deformed to large strains at temperatures of 700 and 800 °C, show a weak but distinct preferred orientation of the crystals evolving with increasing strain. The *c*-axes form a wide maximum approximately perpendicular to the shear plane and along a girdle normal to the shear direction. The *a*-axes are preferentially aligned within the shear plane and form their density maximum almost parallel to the shear direction (Fig. 8). The latter orientation only becomes clear at very large strains ($\gamma = 8$). Similar patterns are reported in the literature for naturally deformed dolomite rocks (Leiss and Barber, 1999) and are interpreted in terms of translation glide on the basal plane (001).

4. Discussion

4.1. Deformation mechanism

Both mechanical measurements and micro-structural observations indicate that fine grained dolomite deformed with a linearly viscous rheology at the experimental conditions (temperatures between 600 and 800 °C and shear strain rates between 1×10^{-6} and 6×10^{-4} s^{-1}). The main deformation mechanism seems to be diffusion creep associated with grain boundary sliding (GBS). GBS was only partially balanced by diffusion and dislocation activity and resulted in the formation and growth of cavities in experiments at temperature $\leq$700 °C, a well-known process in metallurgy and material science (e.g. Pilling and Ridley, 1989), where occurrence of cavities has been associated with a local tensile stress. We interpret the nucleation of such fissures in terms of small, dilatant P-shears promoted by a relatively high pore pressure of CO_2 (around 30 MPa at 700 °C according to the phase diagram of Goldsmith, 1959) due to the equilibrium reaction (7). P-shears are subsidiary synthetic minor faults; they develop oriented at small angle at ($\phi/2$) to the shear zone boundaries, with ϕ being the material internal friction angle (anticlockwise and clockwise to dextral and sinistral sense of shear, respectively). It has been observed elsewhere that P-shears may develop in dilational systems with high fluid pressure (e.g. Moore and Byerlee, 1992; Dahlgren, 2001). The initial geometry depends on the angle of internal friction of the host rock, while the final orientation may result from passive rotation in a simple shear configuration. Thus the cavities would act as passive strain markers. The increasing strain may result in the coalescence of such P-shear cavities, which would then increase in length during their rotation; such a process is referred to as cavitation in metallurgy terminology (Pilling and Ridley, 1989). Experiments performed at temperatures higher than 700 °C did not show any evidence of cavitation, but instead developed a shape preferred orientation of the grains with increasing strain, probably meaning that at this temperature the kinetics of the diffusion processes were enhanced and sufficient to account for the grains sliding past each other, likely due to the CO_2 fluid wetting the grain boundaries and promoting the diffusion movement of elements.

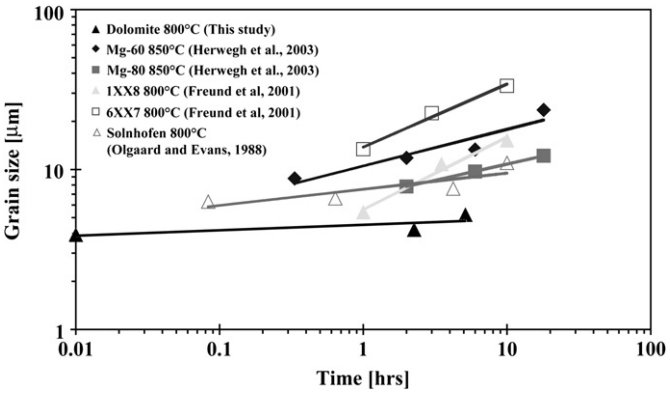

Fig. 11. Compilation of experimental grain growth data for different calcite compositions compared with those obtained on dolomite. The slope of the dolomite trend line is almost flat indicating very slow growth rate.

It is commonly assumed that ductile deformation in a Newtonian regime does not produce a CPO, because diffusion processes do not involve dislocation activity. On the other hand, laboratory studies demonstrated that a complex interaction may arise between the dominant deformation mechanism and the accommodating process in a linearly viscous material. The development of a CPO in a grain size sensitive regime of deformation has been demonstrated, for example, in fine-grained calcite rocks (Schmid et al., 1987; Rutter et al., 1994; Casey et al., 1998) and ice (Goldsby and Kohlstedt, 2001), and could be explained by deformation partitioning between grain boundary sliding and intra-crystalline dislocation creep, with these two mechanism being mutually accommodated.

In the experiments presented here, we could observe a weak but distinct CPO developing with strain, which is substantially different from that of the starting material and could be attributed to glide activity in accordance with what was already reported for naturally and experimentally deformed dolomite.

4.2. Dolomite versus calcite grain growth

The growth rate of synthetic dolomite as observed during deformation (in the diffusion creep field) is reported and compared (Fig. 11) with that described for different studies on calcite in static conditions with different degrees of impurities and on Solnhofen limestone (Olgaard and Evans, 1988; Freund et al., 2001; Herwegh et al., 2003), assuming that grain growth rates in rocks during diffusion creep do not differ from normal static growth rates (Austin and Evans, 2007). As a representative case,

we analyzed the grain size distribution of synthetic dolomite after experiments at 800 °C (i.e. at the temperature conditions in which grain growth should be favoured). Under these experimental conditions, dolomite grain growth (expressed by the slope of the trend line in the grain size versus time plot) is significantly slower than calcite, regardless of the degree of impurity of calcite. These results are in agreement with the experiments of Kronenberg et al. (2003) who reported a much slower growth rate for dolomite than for calcite under high temperature static conditions.

It is therefore likely that a sedimentary sequence composed of alternating calcite- and dolomite-rich layers may undergo a differential grain growth if subject to thermal metamorphism as in the case of a pluton emplacement. The attained grain size will have severe effects on the deformation behaviour of the sequence during subsequent or syn-metamorphic deformation. The deformation mechanism and therefore the rate at which the rock would respond to the applied stresses, will be partitioned according to the grain size of the different materials.

4.3. Dolomite versus calcite flow laws

The results of this study are in broad agreement with concurrent experimental investigation on fine-grained dolomite deformation (Davis et al., in press). Through high temperature, high pressure triaxial tests, the authors found that the high temperature rheology of fine-grained dolomite is nearly linear with a value of stress exponent of 1.28, which compares favourably with the value of $n = 1.3$ in this study.

In both Davis et al.'s study and our work, the determination of the grain size sensitivity of the flow rate is limited by the narrow range of grain size over which the experiment were performed. Nevertheless, our regression yields an m value of 2.6 which supports Davis et al.'s assumption for Coble creep as a dominant diffusion mechanism. Our evaluation of the temperature dependence of diffusion creep differs from that of Davis et al. Their value of $Q = 280 \pm 45$ kJ mol^{-1} is smaller than our $Q = 368 \pm 25$ kJ mol^{-1} from temperature stepping tests. The reasons for these differences may be of geometrical or chemical nature. Geometrical reasons include the different experimental loading set-up used in the two studies and differences in jacket corrections. Chemical differences in terms of major and minor elements concentrations in the starting materials used in the two studies may also contribute to the discrepancy in activation energies.

Comparison and extrapolation of the relative strength of calcite–dolomite rocks can be made using the numerous flow laws reported for experimentally deformed Carrara marble (Schmid et al., 1980), and for a synthetic aggregate of Mg-rich calcite (Herwegh et al., 2003). These cover the possible range of ductile deformation mechanisms for coarse (dislocation creep) and fine-grained (diffusion creep) calcite rocks.

Coarse-grained dolomites deformed in the laboratory are stronger than calcite rocks under all experimental conditions, and flow laws extended to geological conditions indicate that coarse-grained dolomite will be strong relative to calcite-rich units (Davis et al., in press; Bestmann et al., 2000). However, the strength of fine-grained dolomite and calcite aggregates deformed by diffusion creep shows much less contrast in rheology. Field observations that may indicate dolomite deforming by diffusion creep in the case of the Adamello outcrops are:

- The lack of crystallographic preferred orientations (reported in Delle Piane et al., 2007)
- The inferred very high temperatures these marbles underwent (Callegari and Brack, 2002; Matile and Widmer, 1993; Schmid, 1997), which may favour diffusion over dislocation creep.

A comparison between our dolomite flow law and previously established flow laws for calcite rocks predicts a relative strength inversion at high temperatures, with calcite being the weak phase at low temperatures and dolomite being the weak phase at high temperatures (Fig. 12). At laboratory strain rates and for a normalized grain size of 10 μm the rheological inversion occurs for temperatures higher than 700 °C. Extrapolation of the laboratory measurements to a representative tectonic strain rate of 1×10^{-12} s^{-1} and coarsened grain size of 100 μm, predicts such an inversion at temperatures of approx. 550 °C, given that calcite is deforming through dislocation creep and dolomite through grain size sensitive mechanisms. Deformation under high temperature conditions in nature is therefore the essential requirement to observe dolomite behaving in a less competent way than calcite.

5. Conclusions

Cylindrical samples of synthetic fine-grained dolomite were deformed to large strains in torsion experiments. The strength of dolomite was measured as a function of temperature and strain rate, and the mechanical data were used to establish an experimentally based flow law for the high temperature creep of fine grained dolomite.

Between 600 and 800 °C and at shear strain rates ranging from 1×10^{-6} s^{-1} to 6×10^{-4} s^{-1} fine grained dolomite deforms in

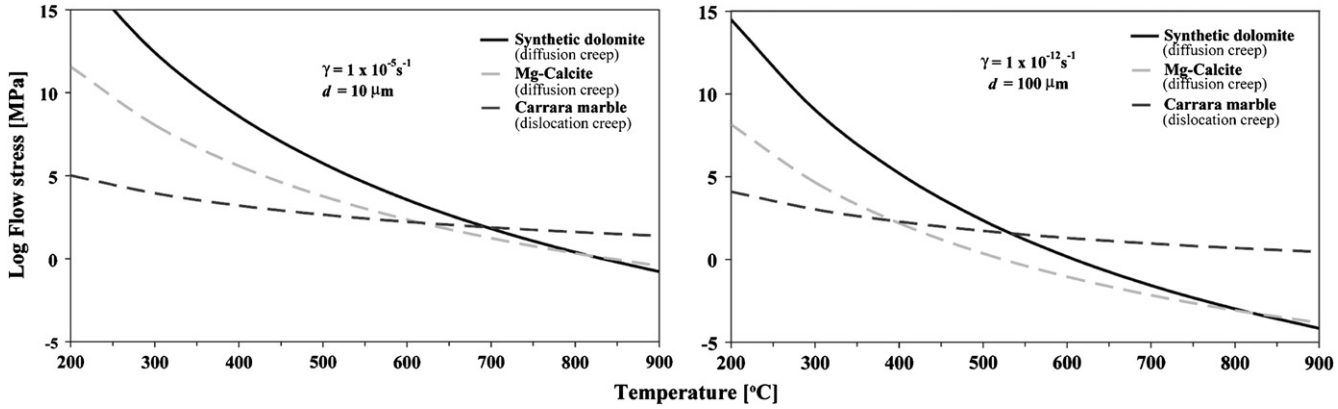

Fig. 12. Flow stress versus temperature (expressed in degrees Celsius) plots comparing the strength of synthetic dolomite, high-Mg synthetic calcite (Herwegh et al., 2003) and Carrara marble (Schmid et al., 1980) at laboratory conditions (left plot). Extrapolation to geological strain rates of 1×10^{-12} s^{-1} for normalized grain size of 100 μm. Under these strain rate and grain size conditions a rheological switch between dolomite deforming by diffusion creep and calcite deforming by dislocation creep is predicted at approximately 600 °C.

a linearly viscous manner, nearly Newtonian, with good evidence for grain boundary sliding being the main deformation mechanism, accommodated by:

1. Dislocation activity resulting in the formation of cavities with a strain dependent geometry and in a weak but distinct CPO
2. Diffusion processes at the highest temperatures investigated, producing flattening of the grains and shape preferred orientation.

The strengths of dolomite and calcite were compared using the available experimentally derived flow laws. A switch in the relative strengths of the two carbonates can be observed under laboratory conditions ($T > 700\,^{\circ}C$) and could be inferred through extrapolation at geologically relevant strain rates for high temperature deformation environments.

These experimental results are consistent with field examples of high temperature, syn-intrusive deformation structures from the contact aureole of the Adamello pluton composed of metamorphosed carbonatic sediments.

Acknowledgements

This work is part of the PhD project of Claudio Delle Piane, ETH grant TH 1/03-3/2704.5. Laboratory equipment and analyses were supported by the NF grant 01066/41-2704.5 and the ETH grant 02150/41-2704.5. R. Hofmann is thanked for the technical support in the laboratory and for the maintenance of the apparatus; Peter Wägli is thanked for assistance with the SEM analyses. Marco Herwegh provided the dolomite powder and Neil Mancktelow the quartz sand used to sinter the starting material. Taras Gerya helped with the data regression methods and Emmanuel Chapron guided us with the particle analysis. This work benefited from discussion with Chris Wilson and Julie Newman we gratefully thank all of them. Careful reviews by Marco Herwegh and Andreas Kronenberg helped clarifying the ideas expressed in this paper.

References

Austin, N.J., Evans, B., 2007. Paleowattmeters: a scaling relation for dynamically recrystallized grain size. Geology 35, 343–346.
Barber, D.J., Wenk, H.R., 1979. Deformation twinning in calcite, dolomite and other rhombohedral carbonates. Physic and Chemistry of Minerals 5, 141–165.
Barber, D.J., Heard, H.C., Wenk, H.R., 1981. Deformation of dolomite single-crystals from 20–800 °C. Physics and Chemistry of Minerals 7 (6), 271–286.
Barber, D.J., Wenk, H.R., Heard, H.C., 1994. The plastic deformation of polycrystalline dolomite: comparison of experimental results with theoretical predictions. Material Science Engineering A175, 83–104.
Barber, D.J., Wenk, H.R., 2001. Slip and dislocation behaviour of dolomite. European Journal of Mineralogy 13, 221–243.
Berger, A., Herwegh, M., 2004. Grain coarsening of contact metamorphic carbonates: effects of second phase particles, fluid flow and thermal perturbations. Journal of Metamorphic Geology 22, 459–474.
Bestmann, M., Kunze, K., Matthews, A., 2000. Evolution of calcite marble shear zone complex on Thassos Island, Greece: microstructural and textural fabrics and their kinematic significance. Journal of Structural Geology 22, 1789–1807.
Brack, P., 1983. Multiple intrusions-examples from the Adamello batholith (Italy) and their significance on the mechanisms of intrusion. Memorie della Societa' Geologica Italiana 26, 145–157.
Callegari, E., Brack, P., 2002. Geological map of the tertiary Adamello batholith (northern Italy). Explanatory notes and legend. Estratto da Memorie di Scienze Geologiche, 54.
Casey, M., Kunze, K., Olgaard, D.L., 1998. Texture of Solnhofen limestone deformed to high strains in torsion. Journal of Structural Geology 20, 255–267.
Dahlgren, S.G., 2001. The nucleation and evolution of Riedel shear zones as deformation bands in porous sandstone. Journal of Structural Geology 23, 1203–1214.
Davis, N.E., Kronenberg, A.K., Newman, J., Plasticity and diffusion creep of dolomite. Tectonophysics, in press. doi: 10.1016/j.tecto.2008.02.002.
Delle Piane, C., Burlini, L., Grobety, B., 2007. Reaction-induced strain localization: torsion experiments on dolomite. Earth and Planetary Science Letters 256, 36–46.
Di Toro, G., Pennacchioni, G., 2004. Superheated friction-induced melts in zoned pseudotachylytes within the Adamello tonalites (Italian Southern Alps). Journal of Structural Geology 26, 1783–1801.
Erickson, S.G., 1994. Deformation of shale and dolomite in the Lewis Thrust-fault zone, Northwest Montana, USA. Canadian Journal of Earth Sciences 31, 1440–1448.
Freund, D., Rybacky, E., Dresen, G., 2001. Effect of impurities on grain growth in synthetic calcite aggregates. Physic and Chemistry of Minerals 28, 737–745.
Goldsby, D.L., Kohlstedt, D., 2001. Superplastic deformation of ice: experimental observations. Journal of Geophysical Research 106, 11017–11030.
Goldsmith, J.R., 1959. Some aspects of the geochemistry of carbonates. In: Abelson, P.H. (Ed.), Researches in Geochemistry, Vol. 1. John Wiley and Sons, New York, pp. 336–358.
Kronenberg, A.K., Davis, N.E., Wheelock, P., Newman, J., 2003. Grain growth kinetics of dolomite and magnesite. Eos, Transactions, American Geophysical Union, 84.
Handin, J., Heard, H.C., Magouirk, J.N., 1967. Effects of the intermediate principal stress on the failure of limestone, dolomite and glass at different temperatures and strain rates. Journal of Geophysical Research 72, 611–640.
Heard, H.C., 1976. Comparison of the flow properties of rocks at crustal conditions. Philosophical Transactions of the Royal Society of London 283, 173–186.
Herwegh, M., 2000. A new technique to automatically quantify microstructures of fine grained carbonate mylonites: two-step etching combined with SEM imaging and image analysis. Journal of Structural Geology 22, 391–400.
Herwegh, M., Xiao, X., Evans, B., 2003. The effect of dissolved magnesium on diffusion creep in calcite. Earth and Planetary Science 212, 457–470.
Higgs, D.V., Handin, J., 1959. Experimental deformation of dolomite single crystals. Geological Society of America Bulletin 70, 245–278.
Leiss, B., Barber, D.J., 1999. Mechanisms of dynamic recrystallization in naturally deformed dolomite inferred from EBSP analyses. Tectonophysics 303, 51–69.
Matile, L., Widmer, T., 1993. Contact metamorphism of siliceous dolomites, marls and pelites in the SE contact aureole of the Bruffione intrusion (SE Adamello, N Italy). Schweizerische Mineralogische und Petrographische Mitteilungen 3, 53–67.
Moore, D., Byerlee, J., 1992. Relationships between sliding behavior and internal geometry of laboratory fault zones and some creeping and locked strike-slip faults of California. Tectonophysics 211, 305–316.
Neumann, E.-R., 1969. Experimental recrystallization of dolomite and comparison of preferred orientations of calcite and dolomite in deformed rocks. Journal of Geology 77, 426–438.
Newman, J., Mitra, G., 1994. Fluid-induced deformation and recrystallization of dolomite at low temperatures along a natural fault zone, Mountain City window, Tennesse. Geological Society of America Bulletin 106, 1267–1280.
Olgaard, D.L., Evans, B., 1988. Grain growth in synthetic marbles with added mica and water. Contribution to Mineralogy and Petrology 100, 246–260.
Paterson, M.S., Olgaard, D.L., 2000. Deformation tests to large shear strains in torsion. Journal of Structural Geology 22, 1341–1358.
Pilling, J., Ridley, N., 1989. Superplasticity in Crystalline Solids. The Institute of Metals, London.
Ramsay, J.G., Huber, M.I., 1983. The Techniques of Modern Structural Geology, 1: Strain Analysis. Academic Press, London.
Rutter, E.H., Casey, M., Burlini, L., 1994. Preferred orientation development during the plastic and superplastic flow of calcite rocks. Journal of Structural Geology 16, 1431–1466.
Schmid, J., 1997. The genesis of white marble: geological causes and archaeological applications. Dissertation, University of Bern, Switzerland.
Schmid, J., Flammer, I., 2002. How grey limestones become white marbles. European Journal of Mineralogy 14, 837–848.
Schmid, S.M., Paterson, M.S., Boland, J.N., 1980. High temperature flow and dynamic recrystallization of Carrara marble. Tectonophysics 65, 245–280.
Schmid, S.M., Panozzo, R., Bauer, S., 1987. Simple shear experiments on calcite rocks: rheology and microfabrics. Journal of Structural Geology 9, 747–778.
Wenk, H.R., Barber, D.J., Reeder, R.J., 1983. Microstructures in carbonates. In: Reeder, R.J. (Ed.), Carbonates: Mineralogy and Chemistry. Reviews in Mineralogy 11. Mineralogical Society of America, Bookcrafters Inc., Chelsea, MI, pp. 301–367.
White, J.C., White, S.H., 1980. High-voltage transmission electron microscopy of naturally deformed polycrystalline dolomite. Tectonophysics 66, 35–54.
Woodward, N.B., Wojtal, S., Paul, J.B., Zadins, Z.Z., 1988. Partitioning of deformation within several external thrust zones of the Appalachian orogen. Journal of Geology 96, 351–361.